2016

Pulses in the Sand: Impulse Response Analysis of Wireless Underground Channel

Abdul Salam
University of Nebraska-Lincoln, salama@purdue.edu

Mehmet C. Vuran
University of Nebraska-Lincoln, mcvuran@cse.unl.edu

Suat Irmak
University of Nebraska-Lincoln, suat.irmak@unl.edu

IEEE INFOCOM 2016 - The 35th Annual IEEE International Conference on Computer Communications
DOI: 10.1109/INFOCOM.2016.7524457

Pulses in the Sand: Impulse Response Analysis of Wireless Underground Channel

Abdul Salam and Mehmet C. Vuran

Cyber-Physical Networking Laboratory
Department of Computer Science & Engineering
University of Nebraska-Lincoln, Lincoln, NE 68588
Email: {asalam, mcvuran}@cse.unl.edu

Suat Irmak

Department of Biological Systems Engineering
University of Nebraska-Lincoln, Lincoln, NE 68583
Email: sirmak2@unl.edu

***Abstract*—Wireless underground sensor networks (WUSNs) are becoming ubiquitous in many areas and designing robust systems requires extensive understanding of the underground (UG) channel characteristics. In this paper, UG channel impulse response is modeled and validated via extensive experiments in indoor and field testbed settings. Three distinct types of soils are selected with sand and clay contents ranging from 13% to 86% and 3% to 32%, respectively. Impacts of changes in soil texture and soil moisture are investigated with more than 1,200 measurements in a novel UG testbed that allows flexibility in soil moisture control. Time domain characteristics of channel such as RMS delay spread, coherence bandwidth, and multipath power gain are analyzed. The analysis of the power delay profile validates the three main components of the UG channel: direct, reflected, and lateral waves. It is shown that RMS delay spread follows a log-normal distribution. The coherence bandwidth ranges between 650 kHz and $1.15MHz$ for soil paths of up to 1m and decreases to 418 kHz for distances above 10m. Soil moisture is shown to affect RMS delay spread non-linearly, which provides opportunities for soil moisture-based dynamic adaptation techniques. The model and analysis paves the way for tailored solutions for data harvesting, UG sub-carrier communication, and UG beamforming.**

I. Introduction

Wireless underground sensor networks (WUSNs) are becoming ubiquitous in many areas including environment and infrastructure monitoring [24], [13], [26], border patrol [2], and precision agriculture [11]. Establishing robust wireless underground communication links between two underground nodes (UG2UG links) or an underground node and a node above the surface (UG2AG links) requires extensive knowledge of the underground (UG) channel characteristics.

In general, performance of a communication system is seriously degraded by multipath fading [14]. Communication in UG channel is affected by multipath fading caused by reflection of electromagnetic (EM) waves in soil and from soil-air interface. Reducing the effects of these disturbances requires characterization of the UG channel. Traditional over-the-air communication channel models cannot be readily used in WUSNs because EM waves in soil suffer higher attenuation than in air due to their incidence in lossy media which consists of soil, water and air, and leads to permittivity variations over time and space with changes in soil moisture [11]. WUSNs are generally deployed at depths which are less than 50 cm [5]. Due to proximity to the Earth surface, a part of the transmitted EM waves propagate from soil to air, then travel along the soil-air interface, and enter the soil again to reach the receiver. These EM waves (*lateral waves* [17]) are a major component of the UG channel.

The analysis of EM wave propagation in underground channel is challenging because of its computation complexity [2]. In [10] and [27], channel models based on the analysis of the EM field and Friis equations have been developed and direct, reflected, and lateral waves are shown to be major contributors of received signal strength. These models provide good approximations when coarse channel measures (e.g., path loss) are concerned but are limited due to the lack of insight into channel statistics (e.g., delay spread, coherence bandwidth) and empirical validations.

Partly unique to the UG channel, there are mainly four types of physical mechanisms that lead to variations in the UG channel statistics, the analyses of which constitute the major contributions of this paper:

1) Soil Texture and Bulk Density Variations: EM waves exhibit attenuation when incident in soil medium. These variations vary with texture and bulk density of soil. For example, sandy soil holds less bound water, which is the major component in soil that absorbs EM waves. Water holding capacity of medium textured soils (silt loam, fine sandy loam, and silty clay loam) is much higher, because of the small pore size, as compared to coarse soils (sand, sandy loam, loamy sand). Medium textured soils have lower pore size and hence, no aggregation and little resistance against gravity [12]. To cover a wide array of soil texture and bulk density variations, we have performed experiments in three distinct types of soils.

2) Soil Moisture Variations: The effective permittivity of soil is a complex number, thus, besides diffusion attenuation, the EM waves also suffer from an additional attenuation caused by the absorption of soil water content. To this end, experiments are conducted with controlled soil moisture variations in an indoor testbed.

3) Distance and Depth Variations: Received signal strength varies with depth of and distance between transmitter and receiver antennas because different components of EM waves suffer attenuation based on their travel paths. Sensors in

WUSN applications are usually buried in topsoil and subsoil layers[1]. Therefore, we have taken measurements for depths of $10-40$ cm with transmitter receiver (T-R) distances of 50 cm to 12 m for UG2UG experiments. Near-field effects of underground antenna for frequency range used in these experiments are within the 30 cm region. In addition, UG2AG experiments are conducted for radii of $2-7$ m with receiver angles of $0°$-$90°$.

4) Frequency Variations: The path loss caused by the attenuation is frequency dependent [9]. In addition, when EM waves propagate in soil, their wavelength shortens due to higher permittivity of soil than the air. Channel capacity in soil is also function of operation frequency. Channel transfer function measurements (S21) are taken to analyze the effects of frequency on underground communication.

In this paper, we present an UG channel impulse response model corresponding analysis based on measured data collected from UG channel experiments with a 250 ps delay resolution. Statistical properties of multipath profiles measured in different soil types under different soil moisture levels are investigated. The results presented here describe: Root mean square (RMS) delay spread, distribution of RMS delay spread, mean amplitude across all profiles for a fixed T-R displacement, effects of soil moisture on peak amplitudes of power delay profiles, mean access delay, and coherence bandwidth statistics. The goal of the measurement campaign and the corresponding model is to produce a reliable channel model which can be used for different types of soils under different conditions. Thus, we have considered several possible scenarios with more than $1,200$ measurements taken over a period of 7 months.

The rest of the paper is organized as follows: The related work is discussed in Section II. Description of UG channel impulse response model is given in Section III. In Section IV, measurement sites and procedures are described. Results and analysis of measured impulse responses are presented in Section V. WUSN communication system design is discussed in Section VI. Paper is concluded in Section VII.

II. Related Work

Wireless communication in WUSNs is an emerging field and few models exist to represent the underground communication. In [27], we have developed a 2-wave model but lateral wave is not considered. In [4], models have been developed but these do not consider underground communication. A model for underground communication in mines and road tunnels has been developed in [24] but it cannot be applied to WUSN due to wave propagation differences between tunnels and soil. We have also developed a closed-form path loss model using lateral waves in [10] but channel impulse response and statistics cannot be captured through this simplified model.

Wireless underground communication shares characteristics of underwater communication [3]. However, underwater communication based on electromagnetic waves is not feasible because of high attenuation. Therefore alternative techniques including acoustic [3] are used in underwater communications. Acoustic technique cannot be used in UG channel due to vibration limitation. In magnetic induction (MI), [18],[25], signal strength decays with inverse cube factor and high data rates are not possible. Moreover, communication cannot take place if sender receiver coils are perpendicular to each other. Therefore, MI cannot be readily implemented in WUSNs.

[1]Topsoil layer (root growth region) consists of top 1 Feet of soil and $2-4$ Feet layer below the topsoil is subsoil.

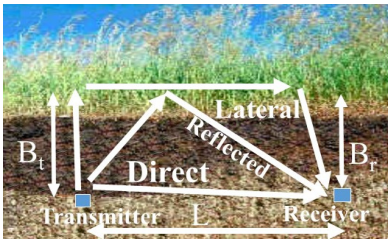

Fig. 1: The three EM waves in an underground channel [10].

To the best of our knowledge, this is the first measurement campaign conducted to analyze and measure the channel impulse response of UG channel and the first work that proposes guidelines for the development of a novel WUSN testbed to improve the accuracy, to reduce the time required to conduct WUSN experiments, and to allow flexibility in soil moisture control.

III. Impulse Response of UG channel

A wireless channel can be completely characterized by its impulse response. Traditionally, a wireless channel is modeled as a linear filter with a complex valued low pass equivalent impulse response which can be expressed as [16]:

$$h(t) = \sum_{l=0}^{L-1} \alpha_l \delta(t - \tau_l) \ , \tag{1}$$

where L, α_l, τ_l are the number of, the complex gains of, and the delays associated with multipaths, respectively.

Schematic view of UG channel is shown in Fig. 1, where a transmitter and a receiver are located at a distance of L and depths of B_t and B_r, respectively [10]. Communication is mainly conducted through three EM waves. First, the direct wave which travels through the soil in line-of-sight from transmitter to receiver. Second, the reflected wave, also travels through the soil, is reflected from the air-soil interface. Third, the lateral wave propagates out of soil, travels along the surface and enters the soil to reach the receiver.

Based on this analysis, the UG channel process can be expressed as a sum of direct, reflected and lateral waves. Hence (1) is rewritten for UG channel as:

$$h_{ug}(t) = \sum_{l=0}^{L-1} \alpha_l \delta(t-\tau_l) + \sum_{d=0}^{D-1} \alpha_d \delta(t-\tau_d) + \sum_{r=0}^{R-1} \alpha_r \delta(t-\tau_r) \ , \tag{2}$$

where L, D, and R are number of multipaths; α_l, α_d, and α_r are complex gains; and τ_l, τ_d, and τ_r are delays associated with lateral wave, direct wave, and reflected wave, respectively.

(a) (b) (c) (d) (e)

Fig. 2: Testbed Development: (a) Testbed box, (c) Packed soil, (b) Layer of gravel at the bottom of the testbed, (d) Antenna placement, (e) Final outlook.

The received power is the area under the profile and is calculated as the sum of powers in all three components in the profile. Accordingly, the received power is given as:

$$P_r = \sum_{l=0}^{L-1} |\alpha_l|^2 + \sum_{d=0}^{D-1} |\alpha_d|^2 + \sum_{r=0}^{R-1} |\alpha_r|^2 \ . \tag{3}$$

The path loss is calculated from the difference of the known transmit power and P_r, and is given as:

$$PL(dBm) = P_t(dBm) + G_t(dBi) + G_r(dBi) - P_r(dBm) \ , \tag{4}$$

where P_t is transmit power, P_r is received power, and G_t and G_r are transmitter and receiver antenna gains, respectively. Antenna effects are included, intrinsically, in the impulse response $h_{ug}(t)$ obtained from the channel transfer function. Traditionally, impulse response of wireless indoor channel is also dependent on antenna properties as power radiated and received in a particular direction is defined by directive gains of transmitter and receiver antennas [21]. In our experiments and analysis, we use omni-directional dipole antennas to observe multipath components in all directions.

Next, we review the metrics derived from the channel impulse response, including excess delay and delay spread. Excess delay is the time delay between the first and last arriving components. Last component is defined by a threshold value in dB relative to the strongest component in the power delay profile (PDP). Typically, a threshold value of -30 dB is used [14],[21]. Mean excess delay (τ) is defined as the first moment of power delay profile and is given as [21]:

$$\tau = \sum_k P_k \tau_k \Big/ \sum_k P_k \ , \tag{5}$$

where P_k is the absolute instantaneous power at the kth bin, and τ_k is the delay of the kth bin.

Root mean square (RMS) delay spread is the square root of the second central moment of the power delay profile and is given as [21]:

$$\tau_{rms} = \sqrt{(\tau^2) - (\tau)^2} \ , \tag{6}$$

where $(\tau^2) = \sum_k P_k \tau_k^2 / \sum_k P_k$, P_k is the absolute instantaneous power at kth bin, and τ_k is the delay of the kth bin. RMS delay spread is a good indicator of multipath spread and it indicates the potential of inter-symbol interference (ISI).

TABLE I: Particle Size Distribution and Classification of Testbed Soils.

Textural Class	%Sand	%Silt	%Clay
Sandy Soil	86	11	3
Silt Loam	33	51	16
Silty Clay Loam	13	55	32

IV. Measurement Sites and Procedures

Measurement are conducted in an indoor testbed (Section IV-A) and field settings (Section IV-B). The measurement procedures are explained in Section IV-C.

A. Indoor Testbed

Conducting WUSN experiments in outdoor settings is a challenging task. These challenges include lack of availability of wide range of soil moisture levels over a short period of time, difficulty of dynamic control over soil moisture, changing soil types, and installation/replacement of equipment. Furthermore, extreme weather and temperature affects make it hard to conduct experiments in all seasons.

To overcome these challenges faced in outdoor environments, an indoor testbed is developed in a greenhouse settings. It is a 100 "x36 "x48 " wooden box (Fig. 2(a)) assembled with wooden planks and contains 90 ft^3 of packed soil. A drainage system is installed in the bottom, and sides of the box are covered with water proof tarp to stop water seepage from sides. Before installation of antennas and sensors, 3 " layer of gravel is laid in the bottom of the box for free drainage of water (Fig. 2(b)) and then soil is placed in the box (Fig. 2(c)).

To monitor the soil moisture level, 8 Watermark sensors are installed on each side of the box at 10 cm, 20 cm, 30 cm and 40 cm depths. These sensors are connected to two Watermark dataloggers. Soil is packed after every 30 cm by using a tamper tool to achieve the bulk density[2] to mimic real-world field conditions. This process is repeated for antenna installation at each depth. Three sets of four dipole antennas are installed (Fig. 2(d)) at the depths of 10 cm, 20 cm, 30 cm, and 40 cm. These sets are 50 cm apart from each other. Final outlook of the testbed is shown in Fig. 2(e).

[2]Bulk density is defined as the ratio of dry soil mass to bulk soil volume including pore spaces.

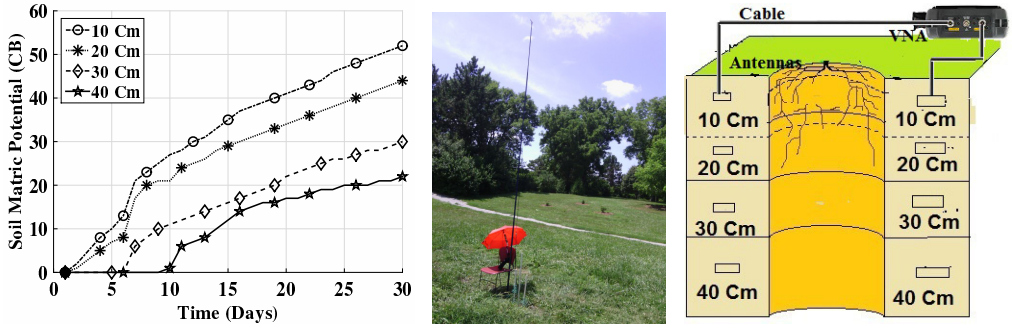

(a) (b) (c)

Fig. 3: (a) Soil moisture (expressed as soil matric potential; greater matric potential values indicate lower soil moisture and zero matric potential represents near saturation condition) with time in silt loam testbed, (b) Outdoor testbed in a field setting, (c) Experiment layout.

We have conducted experiments for two different types of soils in the indoor testbed: silt loam and sandy soil. Particle size distribution and classification of testbed soils is given in Table I. To investigate the effects of soil texture on underground communication, soils selected for use in the testbed have sand contents ranging from 13 % to 86 % and clay contents ranging from 3 % to 32 %. Before starting the experiments, soil is nearly saturated to attain the highest possible level of volumetric water content (VWC) and then measurements are collected as the water potential first reaches to field capacity[3] and then subsequently to wilting point[4]. The changes in soil moisture level with time are shown in Fig. 3(a) for silt loam soil.

B. Field Site

To compare with the results of indoor testbed experiments and conduct underground-to-aboveground experiments, a testbed of dipole antennas has been prepared in an outdoor field with silty clay loam soil (Fig. 3(b)). Dipole antennas are buried in soil at a burial depth of 20 cm with distances from the first antenna as 50 cm-12 m. A pole with adjustable height is used to conduct underground-to-aboveground (UG2AG) experiments with radii of 2 m, 4 m, 5.5 m and 7 m[5] with receiver angles of 0°, 30°, 45°, 60°, 90°.

C. Measurement Procedure

Accurate measurement of channel impulse response can be obtained from frequency domain measurements due to Fourier transform relationship between transfer function and channel impulse response [15]. Accordingly, we have obtained

[3]Plant available water after the drainage of excess water.

[4]Water content level at which water is no more available to plants.

[5]The maximum distance of 7 m is due to the limitations of the antenna cable length for VNA.

TABLE II: Underground Channel Measurement Parameters

Parameter	**Value**
Start Frequency	10 MHz
Stop Frequency	4 GHz
Number of Frequency Points	401
Transmit Power	5 dBm
Vector Network Analyzer	Agilent FieldFox

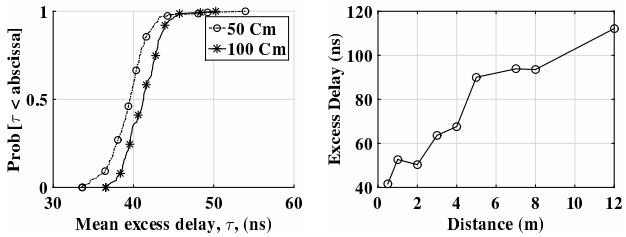

(a) (b)

Fig. 4: (a) Distribution of mean excess delay τ in indoor testbed (silt loam) experiment, (b) Excess delay with distance at 20 cm depth in field (silty clay loam) experiment.

channel impulse by taking frequency domain measurements and then taking inverse Fourier transform. A diagram of the measurement layout is shown in Fig. 3(c). Frequency response of the channel is measured using a Vector Network Analyzer (VNA). VNA-based channel measurements are popular for measuring channel transfer functions in wireless communications and antenna domains [6], [14], [15], [21], [22], [23]. The measurement parameters are given in Table II. The VNA generates a linearly swept frequency signal [20] which is propagated over a frequency range of 10 MHz to 4 GHz. In this range, VNA records 401 complex tones and stores them on external storage for post-processing. The discretized complex channel frequency response H_n is given by [23]:

$$H_n = H(f_{start} + nf_{inc}) \ , \tag{7}$$

where f_{start} and f_{inc} are the start and increment frequencies of the sweep, respectively. H_n is obtained by measuring the reference (R) and input (A) channels and taking the complex ratio, such that $H_n = A_n/R_n$. This process is repeated over the frequency range F_{sweep} at N discrete points, such that $f_{inc} = F_{sweep}/N$. To obtain channel impulse response, the complex frequency data is inverse Fourier transformed. The resulting N point complex channel impulse response has a delay bin spacing of $1/F_{sweep}$ and an unambiguous FFT range of N/F_{sweep}. The measured H_n are windowed using a minimum three term Blackman-Harris window [23] because of its excellent side lobe suppression and relatively wide main lobe width. Before time domain conversion, windowing of H_n is required to avoid $sinc^2$ side lobes associated with

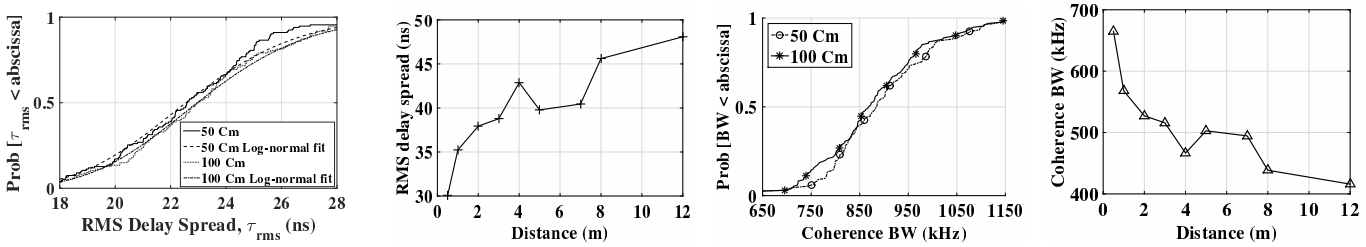

(a) (b) (c) (d)

Fig. 5: (a) Distribution of RMS delay spread, τ_{rms}, for 50 cm and 1 m distance along with log-normal fit over all four depths in indoor testbed (silt loam) experiment, (b) RMS delay spread, τ_{rms}, with distance in field (silty clay loam) experiment, (c) Distribution of coherence bandwidth for 50 cm and 1 m distance in indoor testbed (silt loam) experiment, (d) Coherence bandwidth with distance in field (silty clay loam) experiment.

rectangular nature of frequency sweep [23].

V. Analysis and Results

A. Characterization of UG Channel Impulse Response

Excess delay, mean access delay (5), RMS delay spread (6) [22], [21], [6], and coherence bandwidth in relation to RMS delay spread [15] are the parameters used to characterize the channel. For channel characterization, these parameters are used because system performance is not effected by the actual shape of PDP [22]. In the following, we discuss these metrics and the effects of soil moisture, soil types, distance, and depth on these metrics.

1) Statistics of Mean Excess Delay: Distribution of mean excess delay for 50 cm and 1 m distance over all four depths in indoor testbed (silt loam) experiment is given in Fig. 4(a). Higher mean excess delay can be observed with the increase in T-R separation, which corresponds to an increase of 2 –3ns (8 %). In Table III, statistics for mean (μ) and standard deviation (σ) for the mean excess delay for 50 cm and 1 m distances, and the 4 depths are shown. Higher mean excess delays are also observed as transmitter and receiver are buried deeper. In Fig. 4(b), excess delay is shown as a function of distance at 20 cm depth in field (silty clay loam) experiment. It can be observed that excess delay is increased from 40 ns up to 116 ns as UG communication distance increases from 50 cm to 12 m.

2) Analysis of RMS Delay Spread: Distribution of RMS delay spreads for T-R separations of 50 cm and 1 m in indoor testbed (silt loam) experiment, are shown in Fig. 5(a) with statistical fits. Our analysis shows that empirical distribution of τ_{rms} follows a log-normal distribution and the mean values of 23.94 ns and 24.05 ns and standard deviations of 3.7 ns and 3.4 ns for 50 cm and 1 m distance, respectively. In Table III, statistics for mean (μ) and standard deviation (σ) of the RMS delay spread for 50 m and 1 m distances, and 4 depths are shown. It can be observed from Fig. 5(a) and Table III that RMS delay spread (τ_{rms}) is dependent on T-R separation and burial depth with positive correlation. There is an increase of 2-3 ns (20 %) in RMS delay spread as depth is increased from 10 cm to 40 cm. A 4 ns increase in RMS delay spread can be observed from 10 cm to 20 cm depth at 50 cm distance, which is caused by lateral wave, because at 20 cm lateral wave reaches the receiver after direct wave. At 40 cm, RMS delay spread decreases to 23 ns because lateral wave attenuates more as the burial depth increases. In Fig. 5(b), RMS delay spread is shown as a function of T-R distance at 20 cm depth in field (silty clay loam) experiment. It can be observed that RMS delay spread is increased to 48 ns by increasing distance to 12 m.

The increase in RMS delay spread with depth and distance is contributed by the strong multipaths associated with the lateral and reflected components, since their propagation time differences increase with distance. This increase in RMS delay spread is an important result as it limits the system performance in terms of coherence bandwidth. It has been shown by analysis and simulations that maximum data rate that can be achieved without diversity or equalization is a few percent of the inverse of RMS delay spread [15]. Using this relationship, a coherence bandwidth is established for the RMS delay spread. For our analysis, we have used 90 % signal correlation (1/50 τ_{rms}) as an approximation of coherence bandwidth, because underground channel experiences higher attenuation in soil as compared to terrestrial WSNs, where typically 50 % and 70 % signal correlation values are used to approximate coherence bandwidth.

In Fig. 5(c), distribution of coherence bandwidth for 50 cm and 1 m distance over all depths in indoor testbed (silt loam) experiment is shown. It is observed that the range of coherence bandwidth for UG channel is between 650 kHz to 1.15 MHz for distances up to 1 m. In Fig. 5(d), coherence bandwidth as a function of distance in field (silty clay loam) experiment is shown. It can be observed that coherence bandwidth decreases to 418 kHz (63 %) as communication distance is increased to 12 m. The restriction placed on the coherence bandwidth by the increase in RMS delay spread with distance and depth should definitely be considered in system design but a fine

TABLE III: Mean (μ) and Standard Deviation (σ) in nanoseconds for the mean excess delay and RMS delay spread in indoor testbed (silt loam) experiment.

Depth	Mean Excess Delay τ				RMS Delay Spread τ_{rms}			
	50 cm		1 m		50 cm		1m	
	μ	σ	μ	σ	μ	σ	μ	σ
10 cm	33.53	1.24	36.09	0.80	20.05	2.24	21.94	2.32
20 cm	34.66	1.07	37.12	1.00	24.93	1.64	25.10	1.77
30 cm	35.87	0.72	37.55	0.65	24.84	2.17	25.34	3.41
40 cm	36.43	0.74	40.18	0.94	23.91	2.84	25.62	1.87

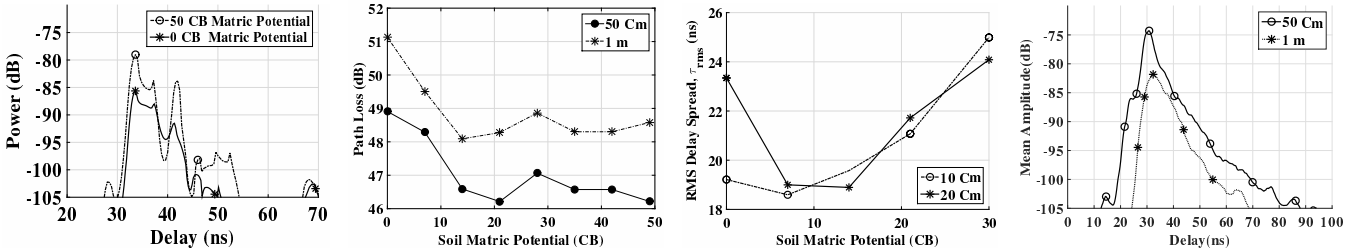

(a) (b) (c) (d)

Fig. 6: Indoor testbed (silt loam) experiment: (a) Power delay profile, (b) Path loss with vs. soil moisture at 10 cm depth, (c) RMS delay spread vs. soil moisture at 50 cm distance, (d) Mean amplitudes of all 50 cm and 1 m profiles across all depths.

design line should not be drawn because of the soil moisture variations, which are discussed next.

3) Soil Moisture Variations: In Fig. 6(a), the effect of soil moisture on amplitudes of a delay profiles is shown for 50 cm distance in indoor testbed (silt loam) experiment. Lower amplitudes can be observed for higher soil moisture (lower soil matric potential (CB)) and this increase is consistent over all delay ranges. Amplitude decrease varies between 5 – 8 dB across the entire PDP.

Water in soil is classified into bound water and free water. Water contained in the first few particle layers of the soil is called bound water, which is strongly held by soil particles due to the effect of osmotic and matric forces [12]. Below these layers, effects of osmotic and matric forces is reduced, which results in unrestricted water movement. EM waves experience dispersion when interfaced with bound water. Since permittivity of soil varies with time due to the variation in soil moisture, wavelength in soil changes which effects the attenuation that waves experience in soil.

In Fig. 6(b), the path loss with change in soil moisture (expressed as soil matric potential[6]) at 50 cm and 1 m distance and 10 cm depth in indoor testbed (silt loam) experiment is shown. Path loss decreases by 3-4 dB (7 %) as soil matric potential changes from 0 to 50 CB (Centibars). In Fig. 6(c), change in RMS delay spread with change in soil moisture at 50 cm distance, 10 cm and 20 cm depth in indoor testbed (silt loam) experiment is shown. From near-saturation to 8 CB, RMS delay spread has decreased first and then increases as soil moisture decreases. This is attributed to water repellency of soil particles where infiltration is slowed momentarily at near-saturation levels. For 10 cm depth, RMS delay spread has increased from 19 ns to 25 ns (31 %) as soil moisture decreases. Similar increase in RMS delay spread with decrease in soil moisture can be observed for 20 cm depth. Low water absorption of EM waves with decrease in soil moisture contributes to increase in τ_{rms} as multipath components exhibit less attenuation.

The variations in amplitudes and path loss with the change in soil moisture lead to changes in coherence bandwidth, optimal system capacity and communication coverage range. Specifically, increase in RMS delay spread with soil moisture decreases coherence bandwidth of the channel, and attenuation is also increased when soil moisture increases. Therefore, underground communication devices should have the ability to adjust their operation frequency, modulation scheme, and transmit power to compensate these changes caused by soil moisture variation. Cognitive radio [1] solutions can be used to adopt parameters based on changing channel conditions.

[6]Greater matric potential values indicate lower soil moisture and zero matric potential represents near saturation condition.

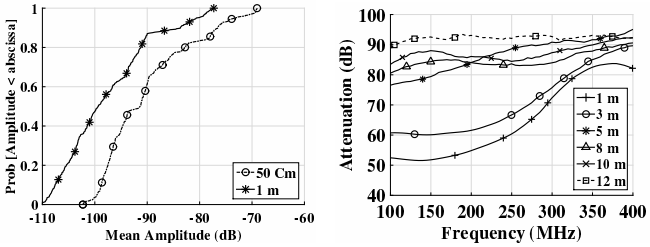

(a) (b)

Fig. 7: Indoor testbed (silt loam) experiment: (a) Distribution function of mean amplitudes at 40 cm depth. Field (silty clay loam) experiment: (b) Attenuation with frequency.

4) Soil Type: Soils are divided into textural classes based on their particle size. To analyze the effects of soil texture, we have measured the channel statistics for silty clay loam, silt loam, and sandy soils. In Table IV, statistics of mean (μ) and standard deviation (σ) for the mean excess delay, RMS delay spread and path Loss for 50 cm and 1 m distances, and 4 depths are shown.

RMS delay spread τ_{rms} in sandy soil is 2 ns higher than silty clay loam, which is 1 ns higher than the silt loam on the average. Similarly, path loss is 4 – 5dB lower in sandy soil as compared to silt loam and silty clay loam. This is due to the lower attenuation in sandy soil. Attenuation of EM waves in soil varies with soil type [9]. Sandy soil holds less bound water, which is the major component in soil that absorbs EM waves. Water holding capacity of fine-textured

TABLE IV: Mean (μ) and Standard Deviation (σ) for the Mean Excess Delay, RMS delay spread and Path Loss for 50 cm and 1 m distances, and 20 cm depth for three soils. Values are in nanoseconds.

Soil Type	Mean Excess Delay				RMS Delay Spread				Path Loss	
	Distance				Distance				Distance	
	50 cm		1 m		50 cm		1 m		50 cm	1 m
	μ	σ	μ	σ	μ	σ	μ	σ		
Silty Clay Loam	34.77	2.44	38.05	0.74	25.67	3.49	26.89	2.98	49 dB	52 dB
Silt Loam	34.66	1.07	37.12	1.00	24.93	1.64	25.10	1.77	48 dB	51 dB
Sandy Soil	34.13	1.90	37.87	0.80	27.89	2.76	29.54	1.66	40 dB	44 dB

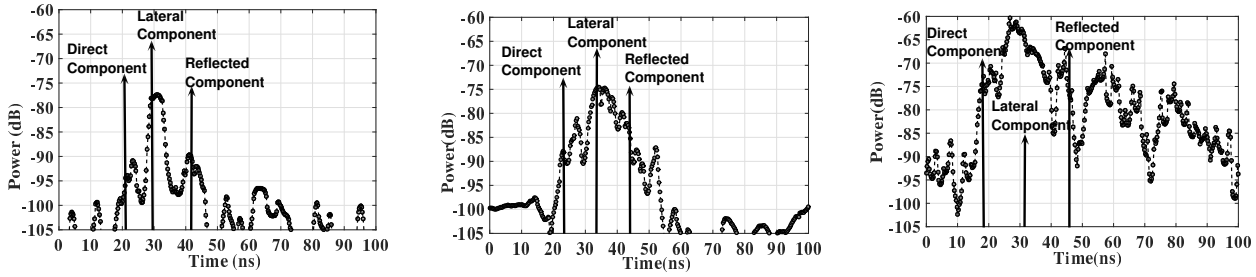

(a) (b) (c)

Fig. 8: Measured impulse response (dotted lines) and impulse response model (solid lines) in: (a) silt loam, (b) silty clay loam soil, and (c) sandy soil.

(silt-loam, silty clay loam) and medium-textured soils (fine sandy loam) is much higher, because of the small pore size (but, greater number of pores), as compared to coarse-textured (sandy, sandy loam, loamy sand) because of larger pore size (but less in number of pores) [12]. Hence the soils containing the highest clay contents suffer more attenuation.

In sandy soil, there is a trade-off between attenuation and RMS delay spread. RMS delay spread τ_{rms} is large due to least attenuated multipath components arriving at the receiver with large delays. On the other hand, overall attenuation is low as compared to silt loam and silty clay loam. Therefore higher SNR can be achieved with moderate coherence bandwidth. Effects of soil texture must be taken into account during design and deployment of WUSNs and optimal system parameters such as communication range and data rates should be selected based on the physical characteristics of the soil.

5) Distance and Depth: Communication in UG channel is effected by depth and T-R separation. However, these impacts are much more severe then over the air communication. In Fig. 6(d), effects of T-R distance are shown in indoor testbed (silt loam) experiment. By increasing the distance from $50\,\text{cm}$ to $1\,\text{m}$, the first component in the $1\,\text{m}$ PDP is delayed by $10\,\text{ns}$. An $8\,\text{dB}$ difference in peak amplitude is observed between profiles at $50\,\text{cm}$ and $1\,\text{m}$. Distribution of mean amplitudes of $50\,\text{cm}$ and $1\,\text{m}$ profiles at $40\,\text{cm}$ depth in indoor testbed (silt loam) experiment is shown in Fig. 7(a). A $9-10\text{dB}$ decrease in mean amplitude can be observed when T-R separation is increased from $50\,\text{cm}$ to $1\,\text{m}$. Peak amplitude of delay profile is decreased by $5\,\text{dB}$ from $10\,\text{cm}$ depth to $40\,\text{cm}$ depth at $50\,\text{cm}$ distance, whereas this decrease in peak amplitude is $20\,\text{dB}$ for $1\,\text{m}$ distance when depth is changed from $10\,\text{cm}$ to $40\,\text{cm}$. Since increase in burial depth increases the path of EM waves in soil, higher attenuation is observed.

EM waves in soil are reflected and attenuated by soil-air interface and suffers diffusion attenuation. Additional attenuation is caused by absorption of waves in soil. Higher attenuation is the limiting factor for communication system design. The attenuation is increased with distance and depth because of reflection effects of lateral wave. At soil-air interface phase of lateral wave is randomly changed, which adds constructive-destructive interference at the receiver.

TABLE V: Speed of the wave in all three soils, calculated by refractive indices n based on particle size distribution of soils given in Table II.

Soil Type	Speed in Soil m/s	% of c	Refractive Index n
Silt Loam	$5.66\text{x}10^7$	18.89	5.28
Sandy Soil	$5.01\text{x}10^7$	16.71	5.98
Silty Clay Loam	$5.67\text{x}10^7$	18.91	5.29

6) Operation Frequency: In Fig. 7(b), attenuation with frequency at different distances of up to $12\,\text{m}$ are presented. Transmitter and receiver depths are set to $20\,\text{cm}$. At $2\,\text{m}$ distance, attenuation increases by $24\,\text{dB}$ when frequency increases from $200\,\text{MHz}$ to $400\,\text{MHz}$. Similarly, for $200\,\text{MHz}$, attenuation is increased from $51\,\text{dB}$ to $92\,\text{dB}$ ($80\,\%$) when distance increases from $50\,\text{cm}$ to $12\,\text{m}$.

Higher frequencies suffer more attenuation because when EM waves propagate in the soil their wavelength shortens due to higher permittivity of soil than the air. Hence, due to less effects of permittivity of soil on lower frequency spectrum, it is more suitable for UG2UG communication as larger communication distances can be achieved. In order to have minimum attenuation, an operation frequency should be selected, for each distance and depth, such that attenuation is minimized. This is important from WUSN topology design perspective because deployment needs to customized to the soil type and frequency range of sensors being used for deployment.

B. Model Parameters and Experimental Verifications

In this section, arrival of multipath components is validated with a schematic of the three model components and model parameters are given. Moreover, the shape of the PDP is presented and with physical interpretations.

Speed of the wave in soil is given as [8] $S = c/n$, where $c = 3\text{x}10^8$ m/s is the speed of light, n is the refractive index of soil $n = \sqrt{\sqrt{\epsilon'^2 + \epsilon''^2} + \epsilon'/2}$, and ϵ' and ϵ'' are the real and imaginary parts of the relative permittivity of the soil.

Arrival time of each of the three components, in nanoseconds, is calculated as follows:

$$\tau_d = (\delta_s/S) + 2 \times (L/S_c)\ , \tag{8}$$

$$\tau_r = 2 \times (\delta_s/S) + 2 \times (L/S_c)\ , \tag{9}$$

$$\tau_l = 2 \times (\delta_s/S) + (\delta_a/c) + 2 \times (L/S_c)\ , \tag{10}$$

where τ_d, τ_r and τ_d are arrival times of the direct, reflected and lateral waves, respectively, δ_s is distance travel by wave in soil, L is the length of the coaxial cable attached to antenna, S_c

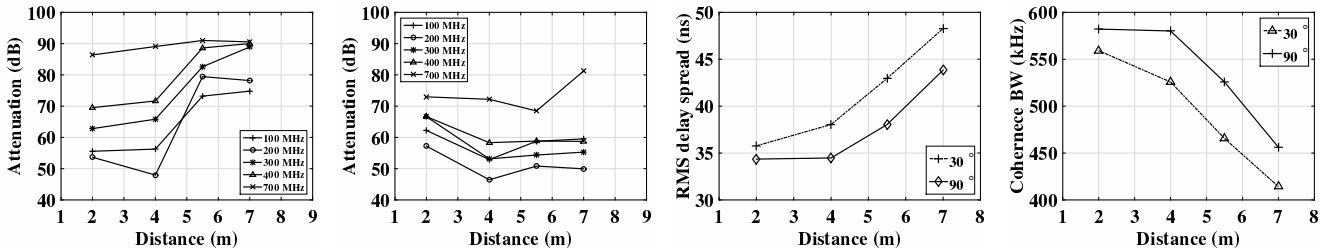

(a) (b) (c) (d)

Fig. 9: Attenuation with distance at different receiver angles (UG2AG) : (a) 0°, (b) 90°, (c) RMS delay spread with distance, (d) Coherence bandwidth with distance.

is the speed of wave in coaxial cable calculated with refractive index of 1.2, S is speed of wave in soil, and c is the speed of light $3x10^8$ m/s.

Based on (8), (9) and (10), the speed of the wave in all three soils is found by calculating the refractive indices n based on particle size distribution and classification of soils given in Table II. The results of these calculations are shown in Table V. In Figs. 8, measured PDPs for three soil types at 40 cm depth is compared with a schematic representation of the 3-wave model for T-R separation of 50 cm. Analysis of arrival time of three components reveals that for 50 Cm distance and all burial depths, lateral waves arrive later than the direct wave except for the 10 Cm depth where lateral wave reaches the receiver first. It can be observed that measurement data shows a strong agreement with the model.

In Table VI, model parameters for peak amplitude, delays, and number of multipaths statistics for direct, lateral and reflected components for three soil types are shown. From Fig. 8 and Table VI, it can be observed that lateral component is the strongest component than the direct and reflected components. This is because direct and reflected components are spherical waves radially outward from the dipole, whereas lateral component is, first, a plane wave that travels upward from the source to the boundary, then travels horizontally as a cylindrical wave, and then travels backward as a plane wave from boundary to point of observation.

VI. WUSN Communication System Design

The presented impulse response model and experiment results provide insight into the statistics of the UG channel. Moreover, the impacts of distance, depth, soil moisture and soil texture on communication channel can be observed. These analyses provide useful insight to system designers in order to obtain desired performance. In this section, we present guidelines, based on results of the presented Underground-to-underground (UG2UG) channel and additional Underground-to-aboveground (UG2AG) channel experiments.

TABLE VI: Model parameters: peak amplitude, delays, and number of multipaths statistics for direct, lateral and reflected components for three soils.

	Silty Clay Loam			Silt Loam			Sandy Soil		
	Distance			Distance			Distance		
	1 m			1 m			1 m		
	Peak α dB	τ ns	N	Peak α dB	τ ns	N	Peak α dB	τ ns	N
Direct Component	-90	18-28	3	-103	15-23	2	-87	11-19	4
Lateral Component	-80	30-40	2	-82	26-43	3	-63	22-45	5
Reflected Component	-91	41-47	2	-94	47-59	4	-70	47-61	6

1) Data Collection: In Figs. 9(a)-9(b), results from UG2AG experiments are shown. This type of channel is used to transfer monitoring data from underground nodes to above ground nodes for subsequent relays and delivery to sink. The underground transmitter is at a depth of 20 cm and the aboveground receiver position is varied at the soil surface at distances of 2 m, 4 m, 5.5 m, and 7 m. Measurements are taken at angles of $0°$, $30°$, $45°$, $60°$, and $90°$ from the transmitter. It is observed that the receiver at the angles of $45°$-$90°$ exhibit the lowest attenuation, $90°$ being the ideal because of no refraction from soil-air interface. Moreover, attenuation does not change for wide range of frequencies and distances.

In Fig. 9(c), and Fig. 9(d), RMS delay spread, τ_{rms} and coherence bandwidth with distance at receiver angles of $30°$ and $90°$ is shown. It can be observed that at the receiver angle of $90°$, RMS delay spread increases by 26% from 34 ns to 43 ns, for an in crease in T-R separation from 2 m to 7 m. Our analysis shows that by changing the receiver position from $90°$ to $30°$, by keeping the the same radius, RMS delay spread is increased by $11\,\%$. This could be explained by refractions from the soil-air interface. Since at $90°$, the wave does not go through refractions, as opposed to the refracted path, to reach the receiver at $30°$. Similar to the UG2UG channel, coherence bandwidth for the UG2AG channel is found to be between 457 KHz to 579 KHz at $90°$, which shows that the soil path is the bottleneck.

2) Underground Beamforming: The dominance of the lateral waves in UG channel as observed in Figs. 8 has important implications in wireless underground communication system design. Lateral component has the potential, via beamforming techniques, to reach at farther underground distances which otherwise are limited (8 m to 12 m) because of higher attenuation in soil. Beam-forming antennas [19] are being used in indoor wireless networks to improve capacity. In UG channel, these multiple antenna arrays can be used to focus the maximum signal energy to exploit the lateral wave. Signal footprint can be tailored by limiting energy radiation in direct and reflected components as these are attenuated most. This type of beam-forming in underground channel could be either adaptive based on effects of frequency and soil moisture on channel, or fixed, based on the soil type, depth and distance of system deployment.

3) Underground OFDM: From an underground communication system design perspective, RMS delay spread and coherence bandwidth findings reported in this paper, for both UG2UG and UG2AG channel, lead to an important conclusion. To achieve high data rates, single carrier approaches may lead to higher bandwidth requirement and use of all available system bandwidth as a single channel for data transmission would result in inter-symbol interference (ISI). Therefore, to achieve high data rates and to overcome ISI problem, Orthogonal Frequency Division Multiplexing (OFDM) [7] can be used for signal transmission, where signal bandwidth of each sub-carrier is less than the coherence bandwidth of underground channel. Moreover, significant performance improvement can be achieved in underground channel when modulation scheme can be designed and adapted based on measured channel impulse response. Such modular adaptation is supported by discrete multi-tone modulation (DMT), a variant of OFDM, by use of set of non-overlapping narrowband carriers and transmission rate is adopted based on each sub-carrier's individual conditions. To develop an optimum strategy and theory to analyze the effects of such technique on underground channel needs to be investigated further.

VII. Conclusion

In this paper, analysis of impulse response of Wireless Underground Sensor Networks (WUSN) channel is presented. A 3-wave based impulse response model of underground channel is developed and validated with measured data. Distribution of mean excess delay and RMS delay spread is determined and it is shown that RMS delay spread is log-normally distributed. Effect of T-R separation on mean amplitudes of power delay profile is showed. We have presented the impact of soil moisture and soil types on RMS delay spread and power gains of delay profiles. It is presented that RMS delay spread increases with increase in soil moisture. It is also showed that coarse-textured soils have larger RMS delay spreads and lower attenuation as compared to fine and medium-textured soils. Coherence bandwidth of UG channel in relation to RMS delay spread is modeled and showed to be less than 1 MHz. Coherence bandwidth findings reveled the use of OFDM for underground channel communication to have ISI free communication and for significant performance improvements. These findings serve as important characterization parameters of UG channel and give guidelines for design of an underground communication system.

VIII. Acknowledgments

This work is supported by a NSF CAREER award (CNS-0953900) and a NSF CyberSEES grant (DBI-1331895).

References

[1] I. F. Akyildiz and et.al., "Next generation/dynamic spectrum access/cognitive radio wireless networks: A survey," *Computer Networks Journal, (Elsevier)*, vol. 50, pp. 2127–2159, September 2006.

[2] I. F. Akyildiz, Z. Sun, and M. C. Vuran, "Signal propagation techniques for wireless underground communication networks," *Physical Communication Journal (Elsevier)*, vol. 2, no. 3, pp. 167–183, Sept. 2009.

[3] A. Bicen, A. Sahin, and O. Akan, "Spectrum-aware underwater networks: Cognitive acoustic communications," *Vehicular Technology Magazine, IEEE*, vol. 7, no. 2, pp. 34–40, June 2012.

[4] H. R. Bogena and et.al., "Hybrid wireless underground sensor networks: Quantification of signal attenuation in soil," *Vadose Zone Journal*, vol. 8, no. 3, pp. 755–761, August 2009.

[5] H. R. Bogena and et.al., "Potential of wireless sensor networks for measuring soil water content variability," *Vadose Zone Journal*, vol. 9, no. 4, pp. 1002–1013, November 2010.

[6] D. Cassioli, M. Win, and A. Molisch, "The ultra-wide bandwidth indoor channel: from statistical model to simulations," *IEEE JSAC*, vol. 20, no. 6, pp. 1247–1257, Aug 2002.

[7] R. W. Chang, "Synthesis of band-limited orthogonal signals for multichannel data transmission," *Bell System Technical Journal*, vol. 45, no. 10, pp. 1775–1796, 1966.

[8] CRC Handbook, *CRC Handbook of Chemistry and Physics*, 95th ed. CRC Press, 2014.

[9] M. Dobson and et.al., "Microwave dielectric behavior of wet soil—Part II: Dielectric mixing models," *IEEE Trans. Geoscience and Remote Sensing*, vol. GE-23, no. 1, pp. 35 –46, January 1985.

[10] X. Dong and M. C. Vuran, "A channel model for wireless underground sensor networks using lateral waves," in *Proc. of IEEE Globecom '11*, Houston, TX, December 2011.

[11] X. Dong, M. C. Vuran, and S. Irmak, "Autonomous precision agricultrue through integration of wireless underground sensor networks with center pivot irrigation systems," *Ad Hoc Networks (Elsevier)*, 2012.

[12] H. D. Foth, *Fundamentals of Soil Science*, 8th ed. John Wiley and Sons, 1990.

[13] H. Guo and Z. Sun, "Channel and energy modeling for self-contained wireless sensor networks in oil reservoirs," *Wireless Communications, IEEE Transactions on*, vol. 13, no. 4, pp. 2258–2269, April 2014.

[14] H. Hashemi, "Impulse response modeling of indoor radio propagation channels," *Selected Areas in Communications, IEEE Journal on*, vol. 11, no. 7, pp. 967–978, Sep 1993.

[15] S. Howard and K. Pahlavan, "Measurement and analysis of the indoor radio channel in the frequency domain," *Instrumentation and Measurement, IEEE Transactions on*, vol. 39, no. 5, pp. 751–755, Oct 1990.

[16] M. N. Islam, B. J. Kim, P. Henry, and E. Rozner, "A wireless channel sounding system for rapid propagation measurements," in *Proc. IEEE ICC' 2013*, Jun. 2013, pp. 5720–5725.

[17] R. W. P. King, M. Owens, and T. T. Wu, *Lateral Electromagnetic Waves*. Springer-Verlag, May 1992.

[18] S. Lin, I. Akyildiz, P. Wang, and Z. Sun, "Distributed cross-layer protocol design for magnetic induction communication in wireless underground sensor networks," *Wireless Communications, IEEE Transactions on*, vol. 14, no. 7, pp. 4006–4019, July 2015.

[19] X. Liu and et.al., "DIRC: increasing indoor wireless capacity using directional antennas," *SIGCOMM Comput. Commun. Rev.*, vol. 39, no. 4, pp. 171–182, Aug. 2009.

[20] M. A. Poletti, "The application of linearly swept frequency measurements," *The Journal of the Acoustical Society of America*, vol. 84, no. 2, pp. 599–610, August 1988.

[21] T. Rappaport, S. Seidel, and K. Takamizawa, "Statistical channel impulse response models for factory and open plan building radio communicate system design," *Communications, IEEE Transactions on*, vol. 39, no. 5, pp. 794–807, May 1991.

[22] A. Saleh and R. Valenzuela, "A statistical model for indoor multipath propagation," *Selected Areas in Communications, IEEE Journal on*, vol. 5, no. 2, pp. 128–137, February 1987.

[23] A. Street, L. Lukama, and D. Edwards, "Use of VNAs for wideband propagation measurements," *Communications, IEE Proceedings-*, vol. 148, no. 6, pp. 411–415, Dec 2001.

[24] Z. Sun and I. Akyildiz, "Channel modeling and analysis for wireless networks in underground mines and road tunnels," *IEEE Transactions on Communications*, vol. 58, no. 6, pp. 1758–1768, June 2010.

[25] X. Tan, Z. Sun, and I. F. Akyildiz, "A testbed of magnetic induction-based communication system for underground applications," *IEEE Antennas and Propagation Magazine*, 2015.

[26] M. J. Tiusanen, "Wideband antenna for underground Soil Scout transmission," *IEEE Antennas and Wireless Propagation Letters*, vol. 5, no. 1, pp. 517–519, December 2006.

[27] M. C. Vuran and I. F. Akyildiz, "Channel model and analysis for wireless underground sensor networks in soil medium," *Physical Communication*, vol. 3, no. 4, pp. 245–254, December 2010.